12. Buick IS, Miller JA, Williams IS, Hand M & Mawby J. 2001. Deep holes in the Centralian Superbasin—SHRIMP zircon constraints on the depositional age of granulites in the eastern Arunta Block. Geological Society of Australia abstracts; 64:13–14.

13. Hoatson DM & Blake DH, eds. 2000. Geology and economic potential of the Palaeoproterozoic layered mafic-ultramafic intrusions in the East Kimberley, Western Australia. Canberra: Australian Geological Survey Organisation, bulletin 246.

14. Cawthorn RG & Meyer FM. 1993. Petrochemistry of the Okiep copper district basic intrusive bodies, northwestern Cape Province, South Africa. Economic Geology; 88:590–605.

15. Maier WD & Barnes S-J. 1999. The origin of Cu sulfide deposits in the Curaçá Valley, Bahia, Brazil: Evidence from Cu, Ni, Se and platinum-group element concentrations. Economic Geology; 94:165–183.

16. Hoatson DM, Wallace DA, Sun S-s, Macias LF, Simpson CJ & Keays RR. 1992. Petrology and platinum-group-element geochemistry of Archaean layered mafic-ultramafic intrusions, west Pilbara Block, Western Australia. Canberra: Australian Geological Survey Organisation, bulletin 242.

➤ Dr Dean Hoatson, Minerals Division, AGSO, phone +61 2 6249 9593 or e-mail dean.hoatson@agso.gov.au 🌏

Rapid mapping of soils and salt stores

Using airborne radiometrics and digital elevation models

JR Wilford, DL Dent, T Dowling & R Braaten

Salinisation of land and rivers is a major problem throughout Australia's agricultural regions. There is a pressing need to map or predict where the salt is, and to understand the nature of salt stores and the conduits through which salt and water are delivered to streams and the land surface.

This article describes a new method (an integrated, catchment-based approach) of modelling natural gamma-ray emissions from the Earth's surface for soil/regolith mapping, and combining the results with topographic indices to delineate salt stores and salt outbreaks in the landscape. Modelled thematic maps produced using this approach allow catchments to be ranked according to their salinity risk, or potential risk, for prioritising remedial management.

Large areas of land in Australia are affected by dryland salinity with more than 240 000 hectares affected in New South Wales and Victoria alone.[1,2] In the next 50 years this area is likely to increase substantially. In Australia, annual damage and loss in production caused by dryland salinity has been estimated at 270 million dollars.[3]
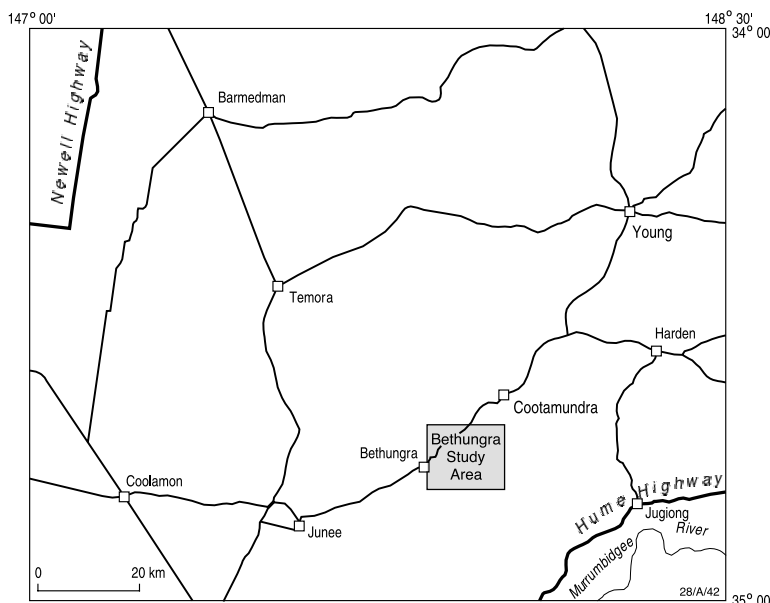
Figure 1. Location of study area within the Cootamundra 1:250 000 map sheet

The salts causing the problem are a common constituent of the regolith and are widespread in Australia. There is consensus that the replacement of natural vegetation by shallow-rooted crops and pastures that use less water has led to increased ground-water recharge and rising ground-water tables. Rising water tables that bring salt to the surface not only affect crops and water quality, but also cause infrastructure damage to towns and transport networks (e.g., roads and railways).

There is an urgent requirement to know where the highest concentrations of salt are, how they are stored in the regolith, and the pathways along which salt is delivered to streams and the land surface.

Study area

The study area (15 by 12 km) is part of the Lachlan Fold Belt of southern Australia, located immediately east of the township of Bethungra, New South Wales (figure 1). Rocks in the area (figure 2) consist of leucocratic granites, rhyolites, rhyodacites and minor siltstones and sandstones.[4] Colluvial and residual clays, sands and minor gravels occur along broad valley floors, footslopes and on rises (9–30 metres relief). The terrain has moderate to high relief (figure 3) with bedrock exposed on steeper
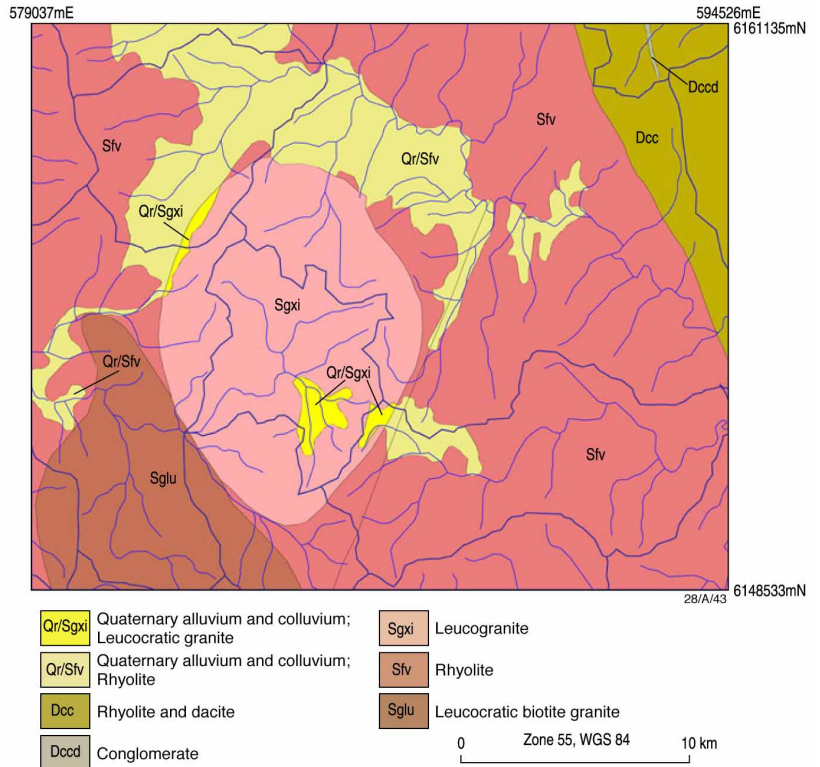
Figure 2. Bedrock lithologies with catchment boundaries and streams overlayed
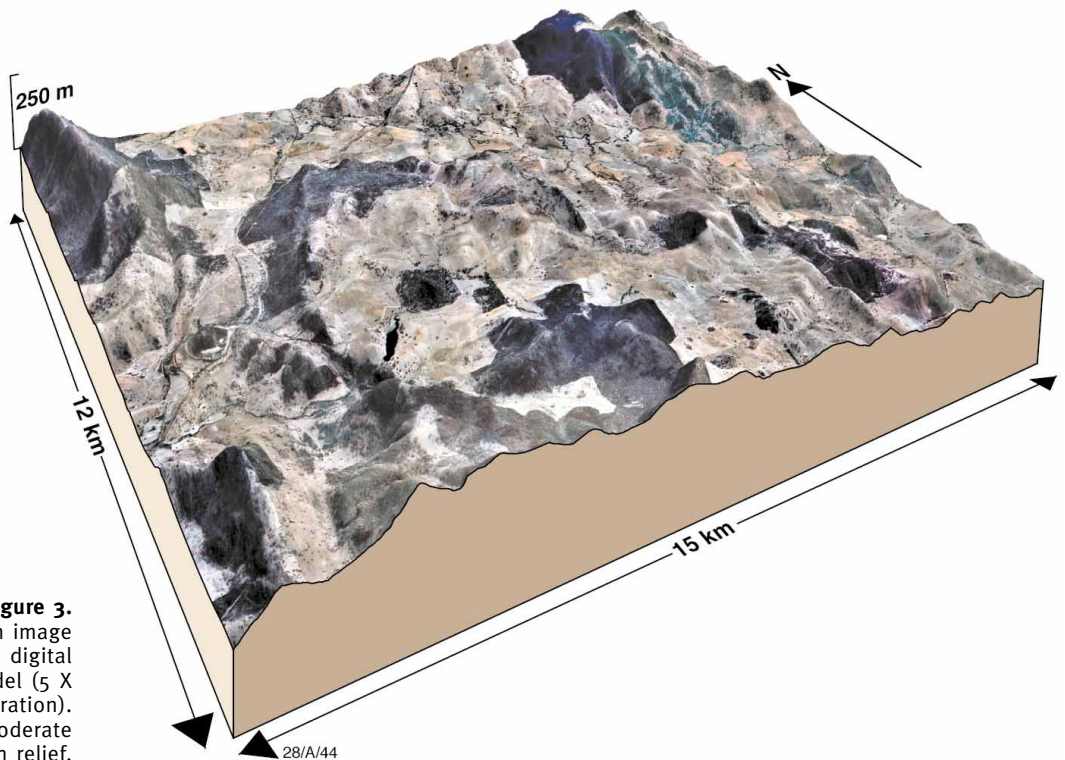
Figure 3. Orthophotograph image draped over a digital elevation model (5 X vertical exaggeration). The area has moderate to high relief.

slopes and ridge tops. The area is typical of erosional landscapes that form part of the south-west slopes of New South Wales. The study complements a geological systems approach to understanding the processes involved in land and water salinisation, that focuses mainly on the interpretation of airborne electromagnetic (EM) data over depositional landforms with a complex regolith cover.[5]

Figure 4. Slope in degrees against potassium (%). Inflection in the curve at around seven degrees separates erosional and depositional processes.

Datasets

Datasets used in the study include airborne gamma-ray spectrometry imagery, a digital elevation model, and catchment and geological polygons.

Gamma-ray spectrometry

Gamma-ray data were clipped from the Cootamundra 1:250 000 map sheet survey flown by AGSO, with 250-metre flight-line spacing and a final grid resolution of 80 metres. Airborne gamma spectrometry measures the natural radiation from potassium (K), thorium (Th) and uranium (U) in the upper 30 centimetres of the Earth's surface. Potassium is measured directly from the radio-element decay of ^{40}K. Thorium and U are inferred from daughter elements associated with distinctive isotopic emissions from ^{208}Tl and ^{214}Bi in their respective decay chains. Since the concentrations of Th and U are inferred from daughter elements, they are usually expressed in equivalent parts per million eU and eTh. Potassium has a much higher crustal abundance than eTh and eU and is usually expressed as a percentage (K%). Gamma-ray spectrometric surveys, therefore, measure the abundance of these radio-elements emanating from topsoil and exposed bedrock.

Gamma-ray spectrometry surveys have been widely used in geophysical exploration, and more recently in soil and regolith mapping.[6–10] The ability of gamma-rays to pass through vegetation to the receiver on the aircraft is an advantage in agricultural regions. Crops and pastures mask the underlying soils, making data from other remote sensors such as Landsat TM difficult to interpret.

Digital elevation model

A digital elevation model of the study area was generated using 1:90 000 aerial photography. Soft photogrammetric techniques were used to create a 50-metre resolution elevation model with one- to five-metre vertical accuracy. Orthophotographic images with a two-metre resolution were also generated (figure 3). The orthophotographs and the DEM were geometrically corrected and warped using differential GPS control points.

Digital elevation models are used widely in terrain classification and modelling. Primary surfaces (e.g., slope, aspect) and secondary or compound surfaces (e.g., wetness index) derived from DEMs are used in hydrological modelling (e.g., surface flow, soil saturation and prediction of discharge and recharge sites) and geomorphological (e.g., erosional and depositional processes) modelling. Dymond et al. demonstrated the use of DEMs in automated land-resource mapping.[11] Broader applications of DEMs for hydrological, geomorpholgical and botanical studies are described by Moore et al.[12]

Vector datasets

Geology polygons were derived from the digital 1:250 000 geological map[4] and catchments were generated from the DEM based on third-order streams.

Modelling gamma-ray spectrometry data

Separating bedrock from regolith responses

Gamma-ray radiation emitted from the ground reflects the chemical composition of the bedrock and overlying soil. Although the gamma-ray signal is received from only the topsoil, the authors reason that in erosional landscapes the divergence of the gamma signal from the bedrock 'signature' reflects soil/regolith characteristics to much greater depths (several metres). This variation from the initial bedrock response is due largely to dilution or preferential enrichment of radio-elements by bedrock weathering and soil formation (e.g., removal of soluble cations and accumulation of sesquioxides that scavenge Th and U). It could also result from the bedrock being buried by transported material (e.g., aeolian dust, colluvium and alluvium). As a general rule, K is lost in solution during bedrock weathering. (K is soluble under most weathering conditions.) However, eTh and eU are more likely to be retained as weathering progresses because they are associated with resistant minerals, clays and iron oxides.
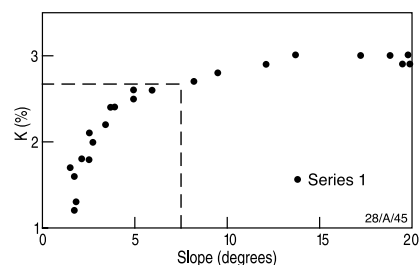
Geomorphic thresholds

GIS techniques have been developed to calculate the gamma-ray bedrock response from different rock-types using a slope grid derived from the DEM. The geology map is used to identify major bedrock units or major lithological/geochemical groups, since the soil response is likely to vary from one bedrock type to another. The bedrock response is differentiated from that of the regolith by plotting the gamma-ray responses against slope (figure 4). Inflection points in the scatter plot correlate with landform thresholds that are used to separate erosional sites from depositional sites. Higher erosion rates on steeper slopes are associated with bedrock materials and thin soils. Here the corresponding gamma-ray response largely reflects the geochemistry of the bedrock. Gentler slopes gain material from above (colluvium) or preserve thicker accumulations of regolith due to lesser rates of erosion. In these parts of the landscape, the corresponding gamma-ray response reflects weathered materials. The relationships between erosion and accumulation and the corresponding gamma-ray response can be used to establish the denudation balance in landscapes.[7]

Once the slope threshold value that partitions erosional landscape facets has been determined, it is used to generate a clipped slope threshold grid. All pixels in the gamma-ray image that correspond with the clipped slope grid are averaged to give a bedrock signature for each rock type. This mean bedrock response is then subtracted from each pixel in the original geophysical channels to generate residual grids for Total Count, K, eTh and eU. The analysis may be performed using lithological units and/or catchments, as regions of interest. However, the units derived from the geology map
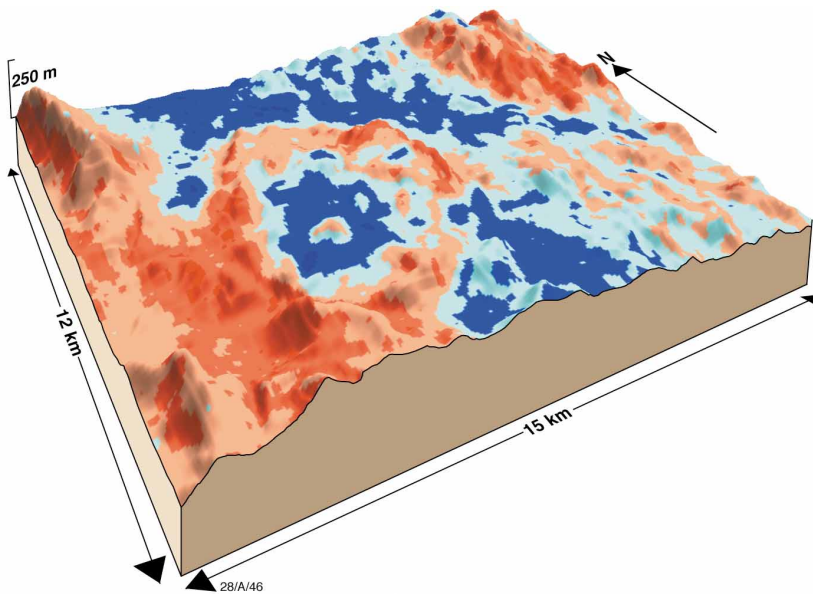
Figure 5. Residual K modelled on geology and catchments. Areas of low divergence from the bedrock mean are shown in reddish hues. These values correspond to exposed bedrock and thin soils. Increasing negative divergence from the bedrock means (shown in green to blue hues) corresponds to clay soils and weathered colluvial sediments. The residual K grid has been draped over a digital elevation model. (5 X vertical exaggeration)
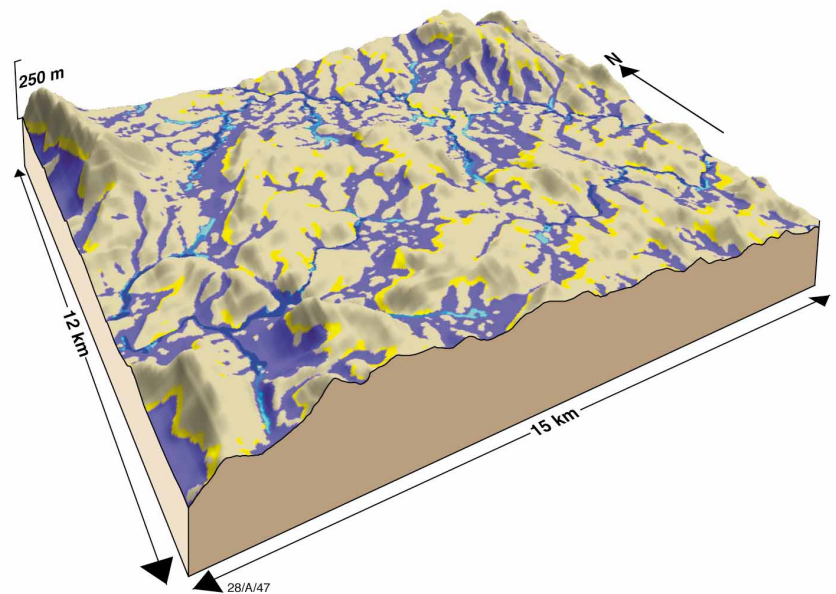
Figure 6. Wetness index derived from FLAG draped over a digital elevation model. Areas in purple and blue show likely surface discharge and local wetness. (5 X vertical exaggeration)

may be inaccurate or have variations due to alteration that is not shown on the map. These effects should be considered when interpreting the image response. Radio-element values centred around the mean bedrock response generally relate to thin soils over bedrock or exposed bedrock. They may also correspond to actively eroded and recently deposited alluvium that still retains the radio-element signature of the bedrock. In erosional landscapes, these sediments tend to be restricted to narrow corridors along streams. Deviation either above or below the mean will largely reflect weathering of bedrock or sediments (figure 5). Where detailed lithology is not known, lithological signatures can still be derived and extrapolated within catchments.

Terrain analysis

Fuzzy Landscape Analysis GIS (FLAG) software was used to derive terrain indices including a landscape position index that can be interpreted as topographic wetness or recharge/discharge zones.[13] FLAG derives and combines a number of topographic indices (scaled from 0–1) from elevation data using the principles of fuzzy set theory. The overall landscape position or wetness index predicts those areas that are both low in their local vicinity (valleys) and low relative to the whole study area. These are sites most likely to exhibit surface wetness and discharge (figure 6). FLAG has been used effectively in salinity studies, identifying waterlogged soils and soil landscape mapping.[14–17]

Results

Mapping residual and transported regolith

Residual modelling of the potassium channel using a greater than seven degree slope geomorphic cut-off value (figure 4) was performed for each catchment and geology unit. The modelled bedrock response was then subtracted from the original K grid to derive a residual K grid (figure 5) with values ranging from -1.8 to 2.4. The bedrock mean has a value of zero. Negative values delineate weathered colluvium and thick clay soils overlying highly weathered mottled saprolite. These soils and saprolite are thickest along broad valley floors and in gently undulating landforms with less than 35 metres local relief. Soil and highly weathered saprolite on undulating

landforms are typically between two to five metres thick, as determined by field observations. Under the broad valley floors, the saprolite is likely to be considerably thicker. Positive values correspond with thin, stony soils (typically less than one metre thick). Because the K signal alone was effective in separating regolith from bedrock materials, the other three channels (Total Count, eTh and eU) were not used in the analysis. The highly weathered mottled saprolite is usually several metres thick. Most of the primary minerals in the saprolite have been weathered, leaving clay and quartz. The saprolite grades into saprock with lower porosity at depth.

Comparing modelled soils with stream salinities

An electrical conductivity (EC) survey of streams, springs and seeps was carried out to test any relationship between salt concentration and the modelled residual K image. Field assessment consisted of 59 stream EC measurements and 31 seep and spring EC measurements.

Measurements were made during April–June 2000 and March 2001. Sample sites included a range of landforms and gamma-ray responses. Some 'noise' would have been introduced to the data because of short-term variation in rainfall amount and intensity over the period of measurement (e.g., variable amounts of base flow and surface flow). Recorded EC measurements are therefore better considered within broad classes than as precise values.

Stream, seep and spring EC values were plotted and overlain on the residual K image (figure 7). Visual inspection showed a good relationship between soils and the EC of streams, springs and seeps. To statistically quantify this relationship, catchment areas for each stream sample point are defined, based on the DEM. The residual K grid value was then computed for each catchment and plotted against EC (figure 8). A relationship between stream EC and the residual K grid was found, with higher stream EC values corresponding to negative residual values.

The EC values ranged from 110 to greater than 3000 µScm. Scatter across the EC values was higher for the more negative residual values. For streams with more positive residual values, the EC values were consistently low (figure 8). The linear relationship between stream EC and the K residual was not exceptionally strong (Pearson's r = -0.58, p <.05).
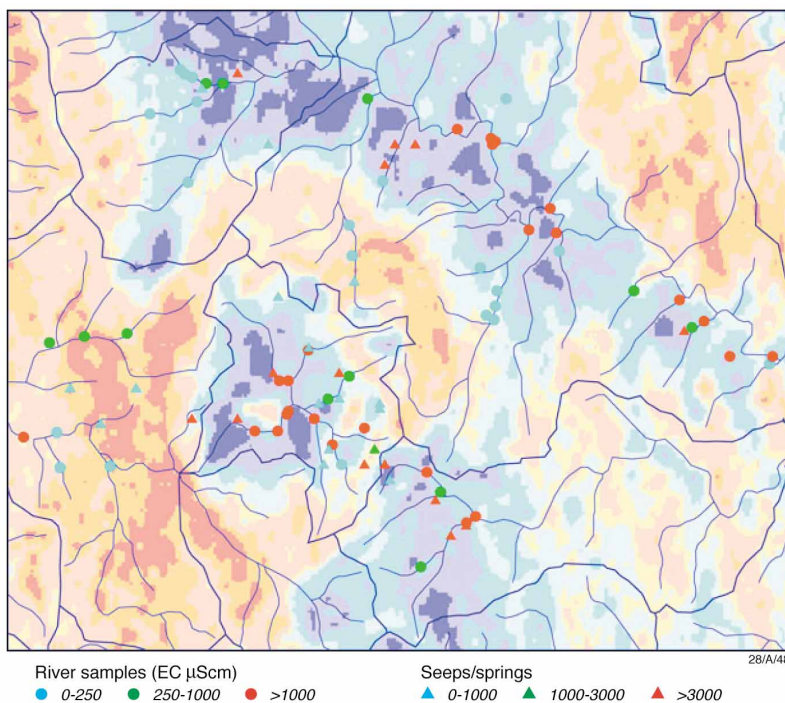
Figure 7. Modelled residual K, with stream EC values superimposed. The soil and bedrock are in red hues, and deeper clay soils and highly weathered saprolite in blue hues.

River samples (EC µScm)   ● 0-250   ● 250-1000   ● >1000
Seeps/springs   ▲ 0-1000   ▲ 1000-3000   ▲ >3000

28/A/48
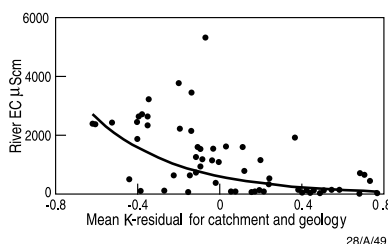
Figure 8. Chart showing residual K with EC measurements from streams and seeps

28/A/49

The relationship was clearer when the streams were grouped into two classes: those draining from areas with highly negative residual values, and those from areas with more positive residual values. There appears to be a natural break at a residual of about 0.37 for these two populations (figure 8). For the 15 stream samples with mean catchment residuals greater than 0.37, the mean EC was 189, the median was 124 and the standard deviation was 218. For the 44 stream samples with residuals less than 0.37, the mean stream EC was 1499, the median 1394 and the standard deviation 1187. A t-test showed a highly significant difference between the two means (p <0.00001).

Combining modelled soils with terrain indices

The wetness grid derived from FLAG was scaled from 0 to 1 and identified areas of high potential surface-water saturation. Values from 0 to 1 showed an increasing wetness trend. The wetness grid was re-scaled from 0 to -1 values and then combined with the K residual grid in which values from 0 to -1 showed increasing negative divergence from the bedrock response (e.g., related to colluvium and thick clay soils). The two grids were combined to produce a final grid with values between -1 and 1 (figure 9). This final grid showed salt stores and the potential discharge or waterlogged sites where one would expect to find saline seeps. A good correlation between independently derived photographic mapped salt scalds[18] and the predicted saline seeps supported the interpretation.

Discussion

Rapid soil mapping

This approach provides a rapid method for mapping and separating deeper regolith and soils from thin soils over bedrock. Colluvial and residual clay soils were delineated using the K residual grid. The method worked best where there was a strong contrast between the radio-element chemistry of the bedrock and the weathered constituents that overlie the bedrock. The K grid was effective over the whole Bethungra area because of the relatively high potassium content of the acid rocks in the area. In areas of contrasting bedrock geochemistry, more complex modelling using all gamma-ray channels is required to effectively map regolith from bedrock materials.[19]

The technique has several advantages when compared with more conventional discrete data classification approaches of interpreting and combining gamma-ray spectrometry and DEM datasets. Firstly the modelled datasets are fuzzy or gradational. This better describes the continuous nature and transitional boundaries of regolith and soil materials and hydrological attributes in landscapes. Secondly, the technique not only identifies soil and regolith materials, but also their associated geomorphic relationships. It is a knowledge-driven approach. This contrasts with a standard classification procedure where it is often difficult to 'unmix' the attributes in the final discrete classes.

Salt stores and EC measurements

In the Bethungra area there was a good correlation between high stream EC and clay distribution in the catchment. This suggests that the clays, and the highly weathered saprolite typically associated with them, are a major source or store of salts. These soils are largely confined to smooth hills with low relief (typically less than 35 metres) and on lower concave slopes and broad valley floors. Catchments with steep rocky hills and relatively higher relief shed predominantly fresh water. Combining these gamma-ray predicted salt stores with a wetness index grid derived from the DEM shows where salt outbreaks might occur, or where the highest salt loads are discharging into the streams. Hence these datasets have the potential to enhance existing GIS-based modelling approaches that use a variety of land attributes and environmental features for salt hazard mapping.[20] Structural controls within saprolite-dominated landscapes that can have an important control on salt movement and surface concentration were not assessed in this study.[21] Future work will incorporate structural analysis (DEM and airborne magnetics) to improve the predictive power of the technique.

Although there was a clear match between EC measurements and predicted salt stores, the overall correlation coefficient was relatively low. This is likely to reflect variable rainfall conditions when field measurements were recorded. Where there is no salt source, there is less opportunity for a stream to acquire a high salt load, resulting in consistently low EC values for streams draining areas with few predicted salt stores. Where streams drain through salt stores, the salt concentration of the stream will depend on the proportion of water derived from surface run-off as opposed to ground water (base flow).

Surface flows have less opportunity to intersect regolith salt stores. As a result, they are fresher and dilute more saline base flow. The partitioning of flow between surface and ground water varies with antecedent soil moisture, rainfall amount and intensity—all of which would have varied between field visits and between streams on the same visit. The variability in surface versus ground water influence on streams is likely to be the reason for the scatter in EC values for streams draining low-residual (high salt-source) areas.
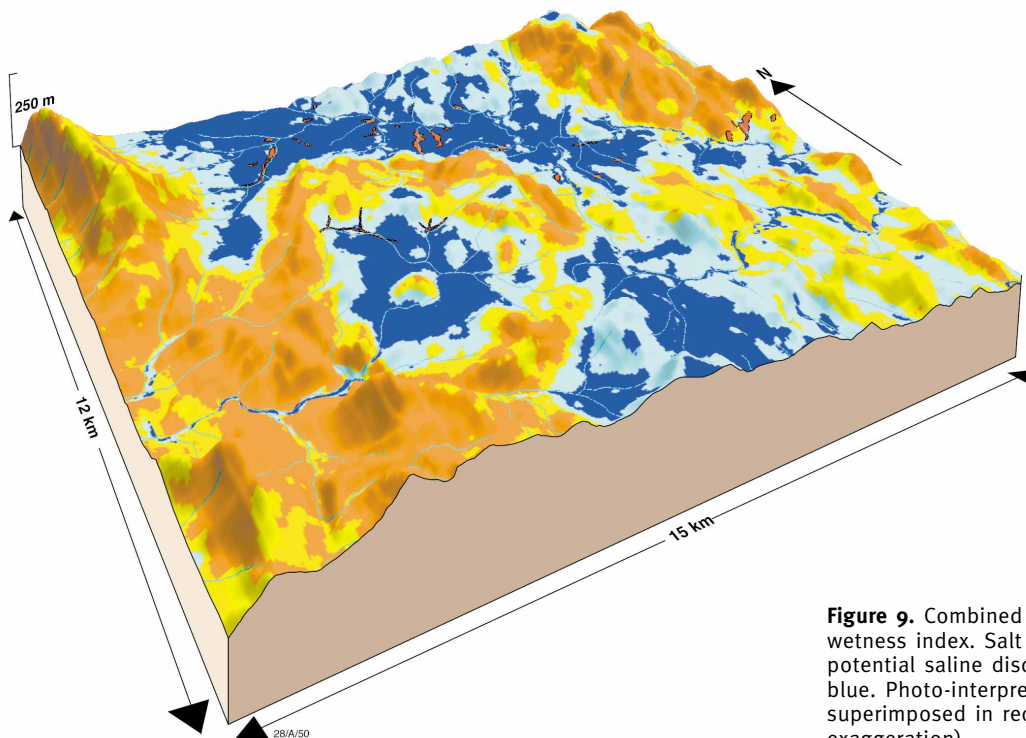
Figure 9. Combined K residual with wetness index. Salt stores and high potential saline discharge sites in blue. Photo-interpreted salt scalds superimposed in red. (5 X vertical exaggeration)

(A) Salt derived from wind blown dust and rainfall

Prevailing wind direction

(B) Partial removal of aeolian material and local reworking into the existing regolith (eg. colluvial and bioturbation processes)

SALTS NOT RETAINED

SALT STORE

28/A/41

Alluvium, sand, clay and minor gravels		
Colluvial reworking of aeolian and weathered bedrock materials. Contains salt		
Aeolian soils containing salt		Saline seeps
Highly weathered saprolite - storing rainwater derived salt and remobilised salt from aeolian soils		Aeolian dust
Saprock - slightly weathered bedrock		Dissolved salts in rainwater

Figure 10. Conceptual model of salt stores and dispersion pathways. **A:** Aeolian dust bringing in salt, probably during arid climatic phases. Salts also derived from rainfall. **B:** Salts stored in the regolith and aeolian deposits. These materials are preserved in geomorphically stable parts of the landscape. Natural water-table fluctuations, and rising water tables caused by tree clearing in areas of high salt storage, result in saline seeps and leakage into streams.

Salt origin and location

Salts are likely to be mainly derived from rainfall and wind-blown dust. Bedrock weathering contributes little to the salts found in the regolith.[22] Highly weathered and porous saprolite probably soaks up atmospheric salts. Work in the Boorowa River catchment showed that streams draining catchments containing thick regolith had consistently higher salt loads than streams incised into fresher bedrock.[22]

Aeolian dust is widely distributed over much of south-eastern Australia.[23–25] These aeolian materials also carried with them considerable amounts of salt, which are now being remobilised.[26,27]

Clay soils in the Bethungra area fit with descriptions of known aeolian sites in south-eastern Australia.[10,28,29] Some components of these clay soils are probably aeolian derived. It is no coincidence that these clays soils and underlying highly weathered saprolite are found in geomorphically stable parts of the landscape where aeolian materials are most likely to be preserved.

The highest salt stores tend to be associated with both aeolian soils and highly weathered regolith, and the lowest associated with thin residual regolith (figure 10). Preliminary 1:5 EC measurements through these more deeply weathered profiles indicate that the salt is in the lower two-thirds of the clay layer and mottled saprolite zone. This suggests that base flow rather than surface flow is the main pathway for salts discharging into streams.

It is debatable whether saline seeps and high stream salinities in the Bethungra area are solely a result of rising ground-water tables caused by post-European native tree clearing. Historical evidence from gold mining records show that ground water in the Temora and Wyalong areas (north-west of the Bethungra study) were highly saline.[30] Studies on the south-eastern Dundas Tablelands in Victoria indicate pre-European salinity based on historical records, past stream flow and bore hydrograph records, and pedological studies (suggesting prolonged seasonal waterlogging).[31] In the Bethungra area it is possible that tree clearing and associated rising ground water has accelerated a natural, near-surface mobilisation of salt in the landscape.

Conclusion

Modelled gamma-ray spectrometry data combined with DEM-derived terrain indices is an effective technique for predicting salt stores and salt outbreaks in erosional landscapes in the Bethungra area. Thematic maps quickly generated by this approach can be used directly in developing farm management plans and in prioritising areas for remedial action. In addition, salt store maps produced by this technique have potential in developing more robust hydrological models for dryland salinity.

More detailed field validation and studies in other areas with contrasting bedrock types, alteration styles and landforms are currently under way to test this application in a wider landscape context. Further work will involve refining the technique, incorporating structural lineament

analysis and applications for depositional areas, and combining the result with other datasets (e.g., climatic grids, land use) using Regolith Expert—a system currently under development in the Cooperative Research Centre for Landscape, Environment and Mineral Exploration.

References

1. Allan MJ. 1993. Victorian dryland salinity database. Melbourne: Centre for Land Protection Research, Department of Conservation & Natural Resources, Victoria.

2. Bradd JM & Gates G. 1996. Dryland salinity in New South Wales: A state perspective. Sydney: Department of Land & Water Conservation, technical report TS95.113.

3. Conacher A & Conacher J. 2000. Environmental planning and management in Australia. Melbourne: Oxford University Press.

4. Warren AY, Gilligan LB & Raphael NM. 1996. Cootamundra 1:250 000 geological sheet SI/55–11. Edn 2. Sydney: Geological Survey of New South Wales.

5. Lawrie KC, Munday TJ, Dent DL, et al. 2000. A geological systems approach to understanding the processes involved in land and water salinisation: The Gilmore project area, central-west New South Wales. AGSO Research Newsletter, May; 32:13–15,26–32.

6. Wilford JR, Pain CF & Dohrenwend JC. 1992. Enhancement and integration of airborne gamma-ray spectrometric and Landsat imagery for regolith mapping—Cape York Peninsula. 9th ASEG Geophysical Conference & Exhibition, Gold Coast, Oct 5–8.

7. Wilford JR, Bierwirth PN & Craig MA. 1997. Application of airborne gamma-ray spectrometry in soil/regolith mapping and applied geomorphology. AGSO Journal of Australian Geology & Geophysics; 17(2):201–216.

8. Dauth C. 1997. Airborne magnetic, radiometric and satellite imagery for regolith mapping in the Yilgarn Craton of Western Australia. Exploration Geophysics; 28:199–203.

9. Cook SE, Corner RJ, Groves RJ & Grealish G. 1996. Application of airborne gamma radiometric data for soil mapping. Australian Journal of Soil Research; 43(1):183–194.

10. Dickson BL & Scott KM. 1998. Recognition of aeolian soils of the Blayney district, NSW: Implications for exploration. Journal of Geochemical Exploration; 63:237–251.

11. Dymond JR & Harmsworth GR. 1994. Towards automated land resource mapping using digital terrain models. ITC Journal; 129–138.

12. Moore ID, Lewis A & Ladson AR. 1991. Digital terrain modelling: A review of hydrological,

geomorphological and biological applications. Hydrologic Processes; 5(1):3–30.

13. Roberts DW, Dowling TI & Walker J. 1997. FLAG: A fuzzy landscape analysis GIS method for dryland salinity assessment. Canberra: CSIRO Land & Water, technical report 8/97.

14. Laffan SW. 1996. Rapid appraisal of ground-water discharge using fuzzy logic and topography. In: Proceedings of 3rd International Conference on Integrating GIS and Environmental Modelling, Santa Fe, Jan 21–25.

15. Dowling TI. 2000. Consulting report: FLAG analysis of catchments in the Wellington region of NSW. Canberra: CSIRO Land & Water, consulting report 12/00.

16. Dowling TI, Summerell G & Walker J. 2001. Soil wetness as an indicator of dryland salinity: A fuzzy landscape analysis GIS. In: Proceedings of the International Symposium on Environmental Software Systems, Banff, May 22–25.

17. Summerell GK, Dowling TI, Wild JA & Beale G. 2001. Fuzzy landscape analysis GIS and its application for determining seasonally wet and waterlogged soils. Australian Journal of Soil Research; in prep.

18. Department of Land & Water Conservation. 1999. Salinity outbreak mapping from aerial photographs. Described in: Littleboy M, Piscopo G, Beecham R, Barnett P, Newman L & Alwood N. 2001. Dryland salinity extent and its impacts. Canberra: National Land & Water Resources Audit, technical report.

19. Wilford JR, Dent D & Dowling T. 2001. Smart interpretation of airborne radiometrics and digital elevation models for salinity mapping. The Land; in prep.

20. Bradd JM, Milne-Home WA & Gates G. 1997. Overview of factors leading to dryland salinity and its potential hazard in New South Wales, Australia. Hydrogeology Journal; 5(1):51–67.

21. George RJ, McFarlane D & Nulsen B. 1997. Salinity threatens the viability of agriculture and ecosystems in Western Australian. Hydrogeology Journal; 5(1):6–21

22. Evans WR. 1998. What does Boorowa tell us? Salt stores and ground-water dynamics in a dryland salinity environment. In: Groundwater sustainable solutions. Melbourne: IAH conference proceedings; 267–274.

23. Butler BE. 1956. Parna and aeolian clay. Australian Journal of Science; 18:145–151.

24. Walker PH & Costin AB. 1971. Atmospheric dust accession in south-eastern Australia. Australian Journal of Soil Research; 9:1–5.

25. Chartres CJ, Chivas AR & Walker PH. 1988. The effect of aeolian accessions on soil development on granitic rocks in south-eastern Australia, II:

Oxygen-isotope, mineralogical and geochemical evidence for aeolian deposition. Australian Journal of Soil Research; 26:17–31.

26. Keifert L. 1977. Characteristics of wind transported dust in eastern Australia. Brisbane: Griffith University, Faculty of Environmental Sciences, PhD thesis.

27. Melis MI & Acworth RI. 2001. An aeolian component in Pleistocene and Holocene valley aggradation: Evidence from Dicks Creek catchment, Yass, New South Wales. Australian Journal of Soil Research; 39(1):13–38.

28. Chen XY. 2001. The red clay mantle in the Wagga Wagga region, New South Wales: Evaluation of an aeolian dust deposit (Yarabee Parna) using methods of soil landscape mapping. Australian Journal of Soil Research; 39(1):61–80.

29. Gatehouse RD, Williams IS & Pillans BJ. 2001. Fingerprinting wind-blown dust in south-eastern Australian soils by uranium-lead dating of detrital zircon. Journal of Soil Research; 39(1):7–12.

30. Andrews EC. 1910. The Forbes-Parkes goldfield. Sydney: Geological Survey of New South Wales, mineral resources 13. In: Wilson & McNally. 1996. Symposium on the Geological Evolution of Eastern Australia. Sydney: Sydney University Consortium of Geology & Geophysics; 71–73.

31. Dahlhaus PG, MacEwan RJ, Nathan EL & Morand VJ. 2000. Salinity on the south-eastern Dundas Tableland, Victoria. Australian Journal of Earth Sciences; 47:3–11.

➤ John Wilford, CRC for Landscape Environment & Mineral Exploration, AGSO, phone +61 2 6249 9455 or e-mail john.wilford@agso.gov.au

➤ Dr David Dent & Robert Braaten, Bureau of Rural Sciences, phone +61 2 6272 5690 or e-mail david.dent@brs.gov.au

➤ Trevor Dowling, Land & Water Division, CSIRO, phone +61 2 6272 4883 or e-mail trevor.dowling@cbr.clw. csiro.au